Journal of Physics B: Atomic, Molecular and Optical Physics

How to administer an antidote to Schrödinger's cat

OPEN ACCESS
IOP Publishing
Journal of Physics B: Atomic, Molecular and Optical Physics
J. Phys. B: At. Mol. Opt. Phys. **55** (2022) 054001 (8pp)
https://doi.org/10.1088/1361-6455/ac5674

How to administer an antidote to Schrödinger's cat

Juan-Rafael Álvarez, Mark IJspeert, Oliver Barter, Ben Yuen[1], Thomas D Barrett[2], Dustin Stuart, Jerome Dilley[3], Annemarie Holleczek[4] and Axel Kuhn*

University of Oxford, Clarendon Laboratory, Parks Road, Oxford OX1 3PU, United Kingdom

E-mail: axel.kuhn@physics.ox.ac.uk

Received 11 October 2021, revised 17 January 2022
Accepted for publication 17 February 2022
Published 17 March 2022

Abstract

In his 1935 Gedankenexperiment, Erwin Schrödinger imagined a box with a cat and a poisonous substance which has a 50% probability of being released, based on the decay of a radioactive atom. As such, the life of the cat and the state of the poison become entangled, and the fate of the cat is determined upon opening the box. We present an experimental technique that keeps the cat alive on any account. This method relies on the time-resolved Hong–Ou–Mandel effect: two long, identical photons impinging on a beam splitter always bunch in either of the outputs. Interpreting the first photon detection as the state of the poison, the second photon is identified as the state of the cat. Even after the collapse of the first photon's state, we show their fates are intertwined through quantum interference. We demonstrate this by a sudden phase change between the inputs, administered conditionally on the outcome of the first detection, which steers the second photon to a pre-defined output and ensures that the cat is always observed alive.

Keywords: quantum feedback, Schrödinger's cat, Hong–Ou–Mandel, single photon sources, cavity QED, atomic fountain

Supplementary material for this article is available online

(Some figures may appear in colour only in the online journal)

1. Introduction

One of the most intriguing principles of quantum mechanics is that of superposition, which states that a quantum system, before being measured, can be interpreted to be in two simultaneous states at once. In his 1935 Gedankenexperiment [1], Erwin Schrödinger illustrated the paradoxical nature of superposition by depicting a cat in a box whose state (dead or alive) is entangled with a vicious device that releases a poisonous substance upon the radioactive decay of an atom which has a probability of 50%. Only upon opening the box for the first time, is it possible to determine the state of the combined system of the cat and the radioactive device; with no decay together with an intact vile and a cat observed alive only half of the time.

The randomness of quantum measurements introduces a fundamental distinction with respect to classical measurements. The process of measurement is central to many open theoretical questions [2], where the measurement induces apparent contradictions between the predictions of quantum mechanics and the appearance of sharp measurement outcomes [3]. In addition, many systems and applications involve a form of quantum control that relies on the quantum nature of measurements [4].

* Author to whom any correspondence should be addressed.
[1] Now at Metamaterials Research Centre, University of Birmingham, Edgbaston, Birmingham, B15 2TT, United Kingdom.
[2] Now at InstaDeep, London, United Kingdom.
[3] Now at Google.
[4] Now at Robert Bosch GmbH, Postfach 13 55, 74003 Heilbronn, Germany.

This poses the question: can a partial measurement of a quantum system be made such that it triggers a sequence of events that coerces the remainder of the system into a desired state? In the example of Schrödinger's cat, observing whether or not the poison has been released normally determines the state of the cat. However, given enough time between poisoning the cat and its actual death, performing such a partial measurement gives one the opportunity to administer an otherwise deadly antidote to a poisoned cat, such that it is always found alive. Such an approach would normally be implemented in the form of a feedback loop, by which a device obtains information about the trajectory of a physical system in order to modify it in real time [5, 6].

In quantum systems, feedback can be of two types: the first, measurement-based quantum feedback, occurs when a measurement outcome defines a subsequent action on the original system. The second, coherent quantum feedback, involves no measurements but provides control using coherent interaction with an auxiliary quantum system.

Both feedback types exist in a range of applications: the generation of amplitude squeezed states in a semiconductor laser [7], the improvement of single-shot phase measurements in quantum metrology [8], the stabilisation of a combined atom-cavity quantum state [9], and the preparation and stabilisation of Fock states in a high-Q microwave cavity with weak measurements [10, 11].

In this work, we take advantage of a measurement-based feedback protocol to deliver a photonic state with a desired property: that of always exiting through the output of a beam splitter of the experimentalist's choosing. Specifically, the feedback process is applied in a time-resolved two-photon quantum interference experiment [12] in which the time span between the first and second photon detection is long enough (~ 500 ns) for a phase change to be applied on the second photon. This allows us to alternate between the behaviours of bosonic and fermionic interference to control the routing of a single photon as desired. The phenomenon of two-photon quantum interference is now pervasive in various different theoretical and experimental settings [13–16]. In particular, the control of the amplitude and phase evolution of the interfering photons has been studied and proven to give rise to pronounced photon–photon correlations in selected time-bins [17].

2. Methods

2.1. Theory

Let us consider two photons arriving simultaneously at the input ports A and B of a beam splitter (BS), as illustrated in the interference box of figure 1. The joint probability of detecting two photons at times t_0 and $t_0+\tau$ at detectors placed at outputs C and D of the BS, respectively, can be written as [12, 18]

$$P_{\text{joint}}\left(t_0,\tau\right)=\left|\hat{E}_D^{+}\left(t_0+\tau\right)\hat{E}_C^{+}\left(t_0\right)\hat{a}_A^{\dagger}\hat{a}_B^{\dagger}\left|0_A0_B\right\rangle\right|^2, \quad (1)$$

where $\hat{a}_A^{\dagger}$ and $\hat{a}_B^{\dagger}$ correspond to the creation operators of a photon in the ports A and B ($\hat{a}_A$ and $\hat{a}_B$ would correspond to the annihilation operators), $\hat{E}_C^{+}+\hat{E}_C^{-}$ and $\hat{E}_D^{+}+\hat{E}_D^{-}$ are the electric field operators at the output ports of the beam splitter, and $|0_A0_B\rangle$ corresponds to the vacuum state on the input ports A and B. In this context, τ can be positive or negative, and $\tau<0$ corresponds to the detector in port D clicking before that in port C. We emphasise that τ is a detection time difference giving rise to a time-resolved Hong–Ou–Mandel (HOM) signal [12, 18], and must not be confused with the photon arrival time difference (Δt) used in many other HOM experiments [19]. Here, we are only interested in the case for which the two photon wavepackets arrive simultaneously ($\Delta t=0$). If $\Delta t\neq 0$, parts of the photon envelope would not overlap, giving rise to random correlations.

The electric field operators can be written as the sum of spatio-temporal functions in distinct modes k, $\zeta_k\left(t\right)=\epsilon_k\left(t\right)\exp\left(-i\phi_k\left(t\right)\right)$:

$$\hat{E}^{+}(t)=\sum_k \zeta_k(t)\hat{a}_k,\hat{E}^{-}(t)=\sum_k \zeta_k^{*}(t)\hat{a}_k^{\dagger}, \quad (2)$$

where $\epsilon_k\left(t\right)$ corresponds to the photon amplitude in mode k and $\phi_k\left(t\right)$ to its phase.

Since the absolute photon detection times are irrelevant, we calculate the joint detection probability as a function of τ only:

$$P_{\text{joint}}\left(\tau\right)=\int_{-\infty}^{\infty}\mathrm{d}t_0 P_{\text{joint}}\left(t_0,\tau\right). \quad (3)$$

Without loss of generality, we consider two linearly polarised photons with a relative polarisation angle θ. In this case, equation (1) can be written as [18]

$$P_{\text{joint}}\left(t_0,\tau\right)=P_{\text{joint}}^{(HV)}\left(t_0,\tau\right)-\cos^2\theta\, F\left(t_0,\tau\right), \quad (4)$$

where

$$P_{\text{joint}}^{(HV)}\left(t_0,\tau\right)=\frac{1}{4}\Big(\left|\epsilon_A\left(t_0\right)\epsilon_B\left(t_0+\tau\right)\right|^2+\left|\epsilon_A\left(t_0+\tau\right)\epsilon_B\left(t_0\right)\right|^2\Big) \quad (5)$$

and

$$F\left(t_0,\tau\right)=\frac{\epsilon_A\left(t_0\right)\epsilon_B\left(t_0+\tau\right)\epsilon_A\left(t_0+\tau\right)\epsilon_B\left(t_0\right)}{2}\times\cos\left(\phi_A\left(t_0\right)-\phi_A\left(t_0+\tau\right)+\phi_B\left(t_0+\tau\right)-\phi_B\left(t_0\right)\right). \quad (6)$$

When both input photons have orthogonal polarisations $\left(\theta=\pi/2\right)$, $P_{\text{joint}}\left(\tau\right)$ can be written as the convolution of their spatio-temporal squared amplitudes, $P_{\text{joint}}\left(\tau\right)=\frac{1}{2}\left(\left|\varepsilon_A\right|^2*\left|\varepsilon_B\right|^2\right)\left(\tau\right)$, rendering the choice of ϕ_A and ϕ_B irrelevant. This is in sharp contrast to the case for which both input photons have parallel polarisations ($\theta=0$), where ϕ_A and ϕ_B become relevant. The expected behaviour of $P_{\text{joint}}\left(\tau\right)$ for the particular case of two photons of perpendicular polarisation with the temporal shape $\epsilon\left(t\right)=\sin^2\left(2\pi t/\delta t\right)$, is shown as a dashed curve in figure 2(a) for $\delta t=400$ ns. The three peaks that are shown in figure 2(a) correspond to the detection of

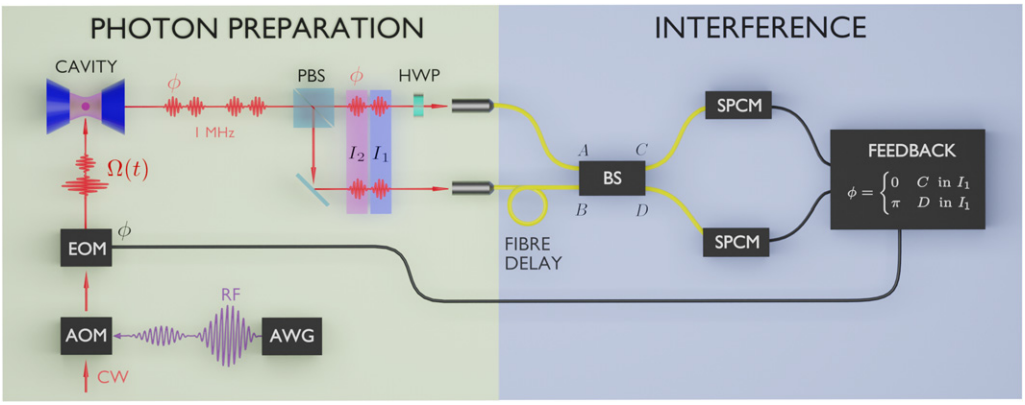

Figure 1. Experimental arrangement: two long, double-hump photons interfere in a beam splitter. Photons are emitted at a repetition rate of 1 MHz from an atomic source driven by a laser pulse controlled by an acousto-optic modulator (AOM), whose phase is changed using an electro-optic modulator (EOM). The AOM pulses are generated by an arbitrary waveform generator (AWG). A delay line with an optical path length of 300 m ensures the simultaneous arrival of two sequentially emitted photons. The emitted photons have such long wave packets, that the first time bin of both photons interferes before the relative phase ϕ of the second photon in the second time bin is set. Furthermore, the emitted photons have random polarisations. Using a polarising beam splitter (PBS), photons are routed into random paths, and two photons simultaneously impinge on the input ports A and B of a beam splitter (BS) in 25% of all possible cases. The relative polarisation between both photons is changed using a half wave plate (HWP). Photons then interfere in the BS and exit through the ports C and D, upon which measurements are performed using single photon counting modules (SPCMs). The outcome of a measurement in the first time bin is used to perform feedback on the value of the phase, ϕ during the second half of the driving pulse.

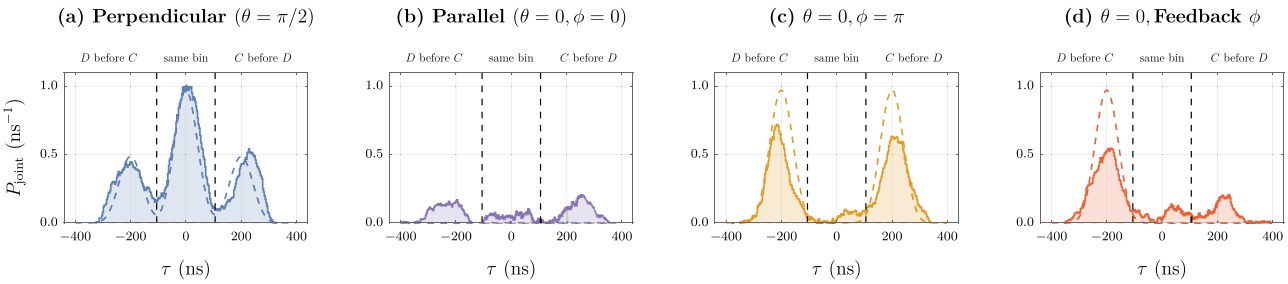

Figure 2. Coincidence probability densities and sliding histograms (whose bin width is larger than its bin separation) showing the theoretical (dashed) and experimental (solid) values for $P_{\text{joint}}(\tau)$. This illustrates the time-resolved HOM interference of two photons under three different conditions. (a) Shows the random routing of photons with perpendicular polarisations, which serves as reference. (b) Shows the interference between indistinguishable photons ($\phi = 0$) with parallel polarisations, resulting in almost no coincidences between the two detectors. Indeed, the theoretical prediction states that $P_{\text{joint}}(\tau) = 0$. (c) Shows the trace obtained for photons with phase shifts of $\phi = \pi$ without feedback. (d) Shows the asymmetric pattern observed under feedback control, where the feedback has prevented (most) correlations in the right satellite peak, steering the second photon to a pre-defined output. This ensures that the cat is always observed alive. The data shown here has been corrected for correlations involving background noise, as explained in the supplemental material.

coincidences in detectors C and D delayed by varying time differences $\tau \in [-400, 400]$ ns.

We subdivide the overall duration of the photons into two distinct intervals (bins) of equal length labelled I_1 (early) and I_2 (late). Additionally, let us assume that, for the photon arriving through A, $\phi_A(t) = 0$ for all times, and that, for the photon arriving through B, $\phi_B(t) = 0$ for $t \in I_1$, and $\phi_B(t) = \phi$ for $t \in I_2$. In the Schrödinger picture [18], the state entering the BS is given by

$$|\Psi_{\text{in}}\rangle = \frac{1}{2}\left(\hat{a}^\dagger_{A1} + \hat{a}^\dagger_{A2}\right)\left(\hat{a}^\dagger_{B1} + \mathrm{e}^{\mathrm{i}\phi}\hat{a}^\dagger_{B2}\right)|0\rangle\,. \tag{7}$$

Here, $\hat{a}^\dagger_{Aj}$ and $\hat{a}^\dagger_{Bj}$ correspond to the photon creation operators in ports A and B in the time intervals I_j, with $j \in \{1, 2\}$, and $|0\rangle$ is the vacuum state in the basis of all the temporal and beam splitter input paths: $|0\rangle = |0_{A1}0_{A2}0_{B1}0_{B2}\rangle$. For the cases $\phi = 0$ and $\phi = \pi$, the theoretical predictions of $P_{\text{joint}}(\tau)$ are shown as dashed curves in figures 2(b) and (c). For the case of figure 2(b), both input photons are identical and feature photon bunching in the output detectors. For this reason, the expected behaviour would not include any coincidences between detectors C and D. In contrast, in figure 2(c) the photon entering through port B acquired a π-phase change from I_1 to I_2. This is the only difference between the two photons. Therefore, if both photons are detected during either I_1 or I_2, the photons are indistinguishable and no correlations are found with $\tau \simeq 0$. However, if the photons are detected in different intervals, the change in phase drives them to different outputs, resulting in a coincidence probability that is twice as large as the orthogonal polarisation case for $\tau = \pm 201$ ns.

Figures 2(b) and (c) exhibit a form that corresponds to a different type of interference between the two photons depending on the value of ϕ. Bosonic ($\phi = 0$) and fermionic interference ($\phi = \pi$) is found with photons either bunching in the same outputs or avoiding each other and giving rise to coincidences, respectively. To see this, consider the following argument, using the Schrödinger picture: the operators after the beam splitter in the output channels C and D in I_j are linked to those before it by the standard unitary relation $\hat{a}^\dagger_{A\,j,Bj} = \left(\hat{a}^\dagger_{Cj} \pm \hat{a}^\dagger_{Dj}\right)/\sqrt{2}$. Therefore, after the beam splitter, equation (7) results in:

$$\begin{aligned}|\Psi_{\text{out}}\rangle = \frac{1}{2\sqrt{2}}\Big(&\left(\hat{a}^\dagger_{C1}\hat{a}^\dagger_{C1} + \mathrm{e}^{\mathrm{i}\phi}\hat{a}^\dagger_{C2}\hat{a}^\dagger_{C2} - \hat{a}^\dagger_{D1}\hat{a}^\dagger_{D1} - \mathrm{e}^{\mathrm{i}\phi}\hat{a}^\dagger_{D2}\hat{a}^\dagger_{D2}\right)\\ &+ \left(\mathrm{e}^{\mathrm{i}\phi}+1\right)\left(\hat{a}^\dagger_{C1}\hat{a}^\dagger_{C2} - \hat{a}^\dagger_{D1}\hat{a}^\dagger_{D2}\right)\\ &+ \left(\mathrm{e}^{\mathrm{i}\phi}-1\right)\left(\hat{a}^\dagger_{C2}\hat{a}^\dagger_{D1} - \hat{a}^\dagger_{C1}\hat{a}^\dagger_{D2}\right)\Big)|0\rangle\,. \end{aligned} \tag{8}$$

Here, $|0\rangle$ is represented in the basis of all the output ports and temporal modes: $|0\rangle = |0_{C1}0_{C2}0_{D1}0_{D2}\rangle$. The first four terms account for both photons arriving at the same detector in the same time bin. These terms lead to the standard boson bunching reported in the canonical HOM effect [19]. The last four terms correspond to cross-correlations between detectors and/or time bins. Unless the single photon detectors are number resolving, it is not possible to measure outcomes where both detections occur at the same detector in the same time bin. By eliminating the terms of the form $\hat{a}^\dagger_{Xi}\hat{a}^\dagger_{Xi}$ and rearranging the terms, the observable sub-state from equation (8) becomes

$$\begin{aligned}\left|\tilde{\Psi}_{\text{out}}\right\rangle = \frac{1}{2\sqrt{2}}\Big(&\hat{a}^\dagger_{C1}\left(\left(\mathrm{e}^{\mathrm{i}\phi}+1\right)\hat{a}^\dagger_{C2} - \left(\mathrm{e}^{\mathrm{i}\phi}-1\right)\hat{a}^\dagger_{D2}\right)\\ &+ \hat{a}^\dagger_{D1}\left(\left(\mathrm{e}^{\mathrm{i}\phi}-1\right)\hat{a}^\dagger_{C2} - \left(\mathrm{e}^{\mathrm{i}\phi}+1\right)\hat{a}^\dagger_{D2}\right)\Big)|0\rangle\,. \end{aligned} \tag{9}$$

In this sub-state, the phase appears explicitly. By setting $\phi = 0$, equation (9) reads

$$\left|\tilde{\Psi}^{(\phi=0)}_{\text{out}}\right\rangle = \frac{1}{\sqrt{2}}\left(\hat{a}^\dagger_{C1}\hat{a}^\dagger_{C2} - \hat{a}^\dagger_{D1}\hat{a}^\dagger_{D2}\right)|0\rangle\,. \tag{10}$$

This state again leads to the canonical HOM effect, yet across the time bins this time. Therefore, both photons arrive at in the same detector, but in separate time intervals. In contrast, setting $\phi = \pi$, equation (9) now gives

$$\left|\tilde{\Psi}^{(\phi=\pi)}_{\text{out}}\right\rangle = \frac{1}{\sqrt{2}}\left(\hat{a}^\dagger_{C1}\hat{a}^\dagger_{D2} - \hat{a}^\dagger_{C2}\hat{a}^\dagger_{D1}\right)|0\rangle\,, \tag{11}$$

which is strikingly different to equation (10), as both photons exhibit fermionic behaviour by arriving at different detectors.

Switching between the bosonic and fermionic behaviour by choice of ϕ allows one to put the system into a pre-defined quantum state conditioned on the random outcome of the first measurement. This is implemented in the form of a feedback mechanism, where a photon detection at either detector in I_1 reveals the required change of ϕ to steer the remaining photon in I_2 to a specific detector. For instance, if detector D clicks in I_1, the second detection would normally occur in detector D, due to the canonical HOM effect. However, as the second halves of the photons have not reached the input ports at the moment of detection, we can instantly change the phase between I_1 and I_2 for one of the incoming photons to change the port in which the second detection occurs. By choosing $\phi = \pi$ and projecting the output state in equation (11) onto the measured state $|0_{C1}1_{D1}\rangle = \hat{a}^\dagger_{D1}|0_{C1}0_{D1}\rangle$ (involving only the first time bin, since the second one has not yet occurred), the state reduces to

$$\left\langle 0_{C1}0_{D1}\left|\hat{a}_{D1}\right|\tilde{\Psi}^{(\phi=\pi)}_{\text{out}}\right\rangle = \frac{1}{\sqrt{2}}\hat{a}^\dagger_{C2}|0_{C2}0_{D2}\rangle\,. \tag{12}$$

This state clearly shows that, when a measurement occurs in I_2, any click will be recorded in detector C. Analogously, if detector C clicks in I_1 and $\phi = 0$ is chosen, both photons are identical in their two halves and any detection in I_2 will always occur at detector C. This reduces the quantum state to

$$\left\langle 0_{C1}0_{D1}\left|\hat{a}_{C1}\right|\tilde{\Psi}^{(\phi=0)}_{\text{out}}\right\rangle = \frac{1}{\sqrt{2}}\hat{a}^\dagger_{C2}|0_{C2}0_{D2}\rangle\,. \tag{13}$$

Again, when a measurement occurs in I_2, any click will be recorded by detector C. Equations (12) and (13) imply that ϕ can be used as a parameter for feedback control, to steer the remaining photon to a desired output.

Returning to equations (3) and (4) with a value of ϕ conditional on the measurement of a photon in I_1, we observe the expected behaviour of $P_{\text{joint}}(\tau)$, as illustrated in figure 2(d). Figure 2(d) shows increased coincidences with $\tau < 0$, for which a detection in D occurs before a detection in C. There are significantly less coincidences with $\tau > 0$, as this would correspond to detector C firing first and detector D second, which cannot occur with an active feedback that always prompts the second detection in C. Figure 2 shows the subset of probabilities for cross-detector correlations only. For this reason, the value $\int P_{\text{joint}}(\tau)\,d\tau$ is bounded by $1/2$. The theoretical curves for same-detector correlations are shown in the supplementary material (https://stacks.iop.org/JPB/55/054001/mmedia).

2.2. Experimental methods

To demonstrate this phenomenon experimentally, we generate photons in an atom-cavity system using a standard V-STIRAP scheme [20] coupling the hyperfine levels of the D_2 line of ^{87}Rb. Specifically, the $|e\rangle = \left|5^2S_{1/2}, F = 1\right\rangle$ and $|g\rangle = \left|5^2S_{1/2}, F = 2\right\rangle$ ground states are coupled in a Λ-scheme to the excited state $|x\rangle = \left|5^2P_{3/2}, F' = 3\right\rangle$ using a driving laser $\Omega(t)$, as illustrated in figure 3. The cavity has a decay rate of $\kappa = 2\pi \times 12$ MHz and a maximum coupling strength of $g_0 = 2\pi \times 15$ MHz. With the system initially prepared in $|e, 0\rangle$, the laser adiabatically drives the system to $|g, 1\rangle$, whereupon the photon is emitted from the cavity mode, leaving the system in $|g, 0\rangle$, decoupled from further evolution. Atoms are loaded into the cavity with an atomic fountain, from a magneto-optic trap (MOT) located directly under the cavity.

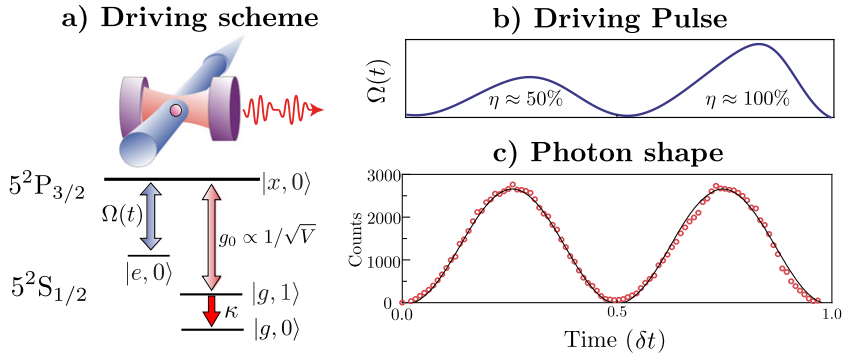

Figure 3. Photon production scheme for the generation of double-hump photons. Figure (a) shows the driving scheme used to generate single photons for a single ^{87}Rb atom inside of an optical cavity, following a coherent STIRAP process $|F=1\rangle \equiv |e\rangle$ and $|F=2\rangle \equiv |g\rangle$ ground states of ^{87}Rb via the virtually excited state $|F'=3\rangle \equiv |x\rangle$ [21]. (b) Shows the pre-calculated [22] pulse necessary for the photon shape to follow the form $\sin^2(2\pi t/\delta t)$, where δt, the photon coherence time, is kept between 400 ns and 450 ns, as can be seen theoretically (solid line) and experimentally (dots) in (c). Our cavity has a decay rate of $\kappa = 2\pi \times 12$ MHz and coupling strength of $g = 2\pi \times 15$ MHz.

The spatio-temporal profile $\zeta(t)$ of the emitted photons can be directly controlled by shaping the driving pulse [21] using an acousto-optic modulator (AOM). For our purposes, it is most crucial that the phase of the driving laser, which we control via a separate electro-optic modulator (EOM), is directly mapped to the phase of the emitted photon. Figure 3(b) shows the driving pulse shape and figure 3(c) the resulting doubly-humped photon profile, evenly distributed across two 200 ns time-bins, for a total coherence time of $\delta t = 400$ ns.

The experimental sequence for the production of photons is as follows: photons are emitted at a repetition rate of 1 MHz, with approximately 400 ns of the cycle used for the production of a single photon. The remaining 600 ns of the cycle are used to optically repump the atom to $|e\rangle$ to repeat the process. The photon production and repumping timings can be changed at will. After being emitted, the photons impinge on a polarising beam splitter (PBS), and are randomly routed into two paths, one of which incorporates a fibre loop of 300 m of optical path length to induce a 1 μs delay. This ensures that a pair of subsequently emitted photons arrives simultaneously at the beam splitter, which is the only case of interest. A half wave plate (HWP) sets the relative polarisation of both photons.

Note from figure 3(c), that the first halves of the emitted photons span 60 m ($\sim$ 200 ns), despite the optical path length between the cavity and the detectors being only 1.5 m or 301.5 m, depending on the path taken. This means that the first time interval of the two photon state is already being measured before the second half of the second photon leaving the cavity (travelling along the shorter path) has been fully generated. The length of the interfering photons is sufficient for a feedback loop to alter the phase ϕ of the second half of the photon under production, conditioned on the measurement outcome within the first time interval (figure 1).

The feedback is implemented using a home-built circuit controller and single photon counting modules (SPCMs) with a quantum efficiency of 60%–65% and a resolution of <300 ps (Excelitas SPCM-AQRH-780-14-FC). The total feedback loop latency, from the EOM via the cavity to the SPCM, then back to the EOM via the controller circuitry is 97.0 ± 0.2 ns. Therefore, a conditioned phase change cannot be realised in time if a photon detection in I_2 occurs less than 97 ns after a detection in I_1. The resulting error rate is limited to 0.2% for a $\sin^4(t)$ photon intensity envelope. All photon counts are recorded with 81 ps accuracy using a qutools quTAU time-to-digital converter (TDC). Detections within the 400 ns photon window are further processed for a dark count correction for each SPCM. A detailed description on the error rates, time budgets, the implementation of the logical feedback circuit and background correction is provided in the supplemental material.

3. Results

There are two different ways to look at the measured data. One has been discussed previously and corresponds to figure 2, which shows the coincidence probability as a function of the time-difference between two detections. However, our main interest is whether both detections are registered within the same or opposite time intervals (I_1 and I_2). Therefore, the same data can be represented in a cross-correlation diagram (figure 4) showing the four possible values of the coincidence probability between detectors C and D firing in either I_1 or I_2. In contrast to figure 3, this allows to further differentiate between coinciding detections in I_1 and I_2.

The cross detection probability of interfering photons with perpendicular polarisations is shown in figure 2(a). This gives rise to the random routing of the simultaneously arriving photons, such that the resulting time-resolved coincidence rate yields the autocorrelation function of the photons' intensity profile. The cross-correlations are depicted in figure 4(a). For the case of photons with orthogonal polarisations, these are identical and theoretically equal to $1/8$.

For photons with parallel polarisations, the cross correlation probability is shown in figure 2(b) for $\phi = 0$. This measurement follows the predictions of photon bunching in the canonical HOM effect, for which we expect no coincidences. Photons bunch in the same output regardless of the actual detection time. Thus, the probability of cross channel detections is expected to be zero for all time differences (figure 4(b)).

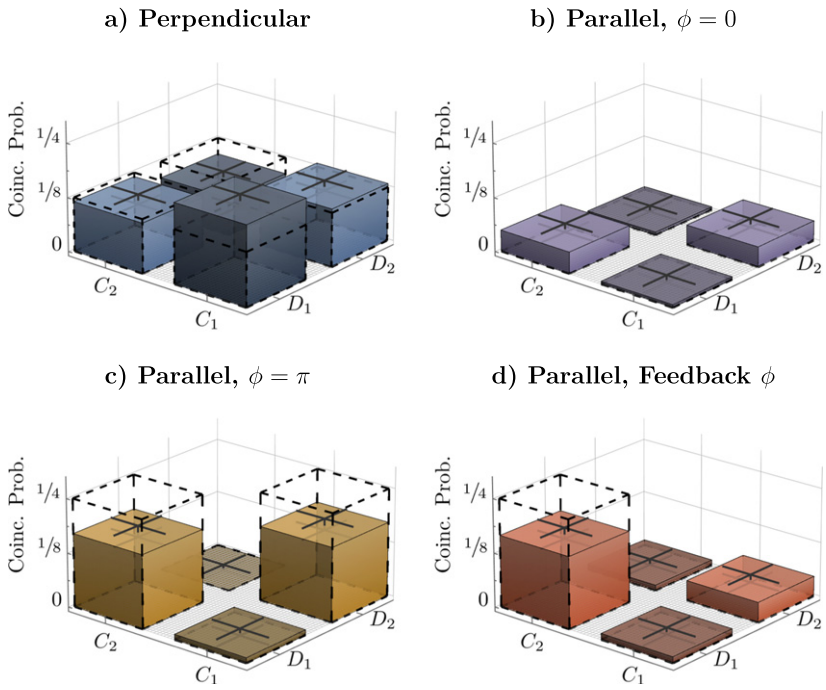

Figure 4. The correlations from figure 2 are now shown according to the exact detector-time-bin detections. In (a), an increased number in the correlations between C_1 and D_1 with respect to C_2 and D_2 is explained due to a larger number of photons in the first time bin, as shown in the supplementary material. In (d), we observe an increase in the correlations between C_2 and D_1 with respect to (a). This implies that a detection in D in I_1 has been used to steer the measurement of a photon in I_2 to C, and serves as a demonstration that the second photon is sent to a pre-defined output state, i.e., the cat is always observed alive. A limitation in visibility is evident when comparing the data to their theoretical values, shown dashed. The data shown here has been corrected for correlations involving background noise, as explained in the supplementary material. The crosses in the middle of the columns indicate the error obtained from a propagation of the statistical $\sqrt{N}$ noise affecting the underlying correlation counts.

Figure 2(c) shows the cross detection probability for photons with parallel polarisations when $\phi = \pi$. In this case, the photons antibunch (i.e., they are found in different output channels if detected in different time intervals). The maximum probability to find photon–photon correlations occurs at $\tau = \pm\delta t$, where δt is the length of the photons. This maximum probability is twice the reference value of figure 2(a), which is in accordance with the cross-channel detections shown in figure 4(c). Nonetheless, the likelihood of correlated photon detections in the same time interval is close to its theoretical value of zero.

Finally, the cross detection probability shown in figure 2(d) represents the case of active feedback on ϕ, for which we expect any photon recorded in I_2 be detected at C. Therefore, the number of 'D before$C$' correlations reaches a maximum while we barely see any 'C before$D$' correlations, as shown in figure 4(d). Our experimental results demonstrate that classical feedback control of a quantum excitation spanning multiple systems (RF pulse driving AOM $\rightarrow$ driving laser $\rightarrow$ atom $\rightarrow$ cavity $\rightarrow$ quantum field modes) can be achieved, resulting in a photonic state with the property of always exiting through the same output of a beam splitter.

Some differences between theoretical expectations and experimental results are visible in figures 2 and 4. These can be attributed to a partial loss of coherence or depolarisation of the interfering photons, most evident from the presence of correlations in the side lobes of figure 2(b). The mutual coherence between photons is often characterised by the HOM visibility, defined as

$$V_{\mathrm{HOM}} = 1 - \frac{N_{\parallel}}{N_{\perp}}, \tag{14}$$

where $N_{\parallel}$ and $N_{\perp}$ are the total number of correlations observed for interfering photons with parallel and perpendicular polarisations, respectively. Using the results obtained with $\phi = 0$ for $N_{\parallel}$ we find $V_{\mathrm{HOM}} = 0.78 \pm 0.04$. However, we measure a reduced visibility of $V_{\mathrm{ref}} = 0.61 \pm 0.04$ if we restrict our analysis to those correlations with detections across time intervals I_1 and I_2. This serves as a reference for all effects discussed here, as these affect only the correlations across both time intervals.

The visibility under phase control upon switching between $\phi = 0$ and $\phi = \pi$ reads

$$V_{\phi} = \frac{N_{\pi} - N_0}{N_{\pi} + N_0}, \tag{15}$$

where N_0 and N_{π} represent the coincidence counts between pairs of photons with relative phase shifts of $\phi = 0$ and π, respectively. Again, we only count coincidences across I_1 and I_2, and find $V_{\phi} = 0.56 \pm 0.06$, in agreement with V_{ref} within error bars. This validates the robustness of the phase switch as no further loss of coherence is induced[5].

[5] V_{ref} and V_{ϕ} are expected to yield the same value, assuming $N_{\parallel} = N_0$ and $N_{\perp} = (N_0 + N_{\pi})/2$ due to the random splitting of photons.

Since the feedback relies on a conditional phase switch, we quantify its visibility by comparing coincidence counts between intervals where a measurement in D occurs before one in C (N_{D1C2}), and vice-versa (N_{C1D2}):

$$V_{\text{feed}} = \frac{N_{D1C2} - N_{C1D2}}{N_{D1C2} + N_{C1D2}}. \tag{16}$$

For our experiment, we find $V_{\text{feed}} = 0.56 \pm 0.06$, which is identical to V_ϕ and equally within error bars of V_{ref}. We therefore conclude that the feedback works as expected, without introducing any loss of coherence.

4. Discussion

We have demonstrated a technique for steering the measurement of a quantum superposition towards a definitive result, a result which can be interpreted as ensuring that Schrödinger's cat is always observed alive. This was achieved by using a feedback mechanism that enforces either bosonic or fermionic behaviour on interfering photons with long coherence lengths.

We emphasize that a classical interpretation of the described experiment fails. Classically, one might expect the feedback control to be successful only when the first detection corresponds to the photon in the delay arm. Otherwise, if the first detection was of the photon in the short arm, the phase change of the driving laser would have no effect (as the photon under generation has already been detected). In a classical description, one would expect a random routing of the second photon regardless of the phase switch, and a reduction of the feedback visibility to zero, which is clearly not the case.

This result constitutes an elementary step towards introducing active control into processes such as quantum random walks and optical networks [23]. Generalisations of the technique demonstrated here are suitable candidates in photonic switchyards requiring multiple photon streams for studying multi-mode interferometry [24], where the deterministic routing of photons would be performed using feedback operations.

Acknowledgments

This work has been funded by the European Union Horizon 2020 (Marie Sklodowska-Curie 765075-LIMQUET), as well as EPSRC through the quantum technologies programme (NQIT hub, EP/M013243/1). JRA acknowledges Alejandra Valencia, David Guzmán, Ezra Kassa and Sebastián Murgueitio Ramírez for useful discussions.

We dedicate this paper to the memory of Bruce W Shore, who sadly passed away on 9 January 2021. Bruce inspired us to keep questioning the fundamental principles of the light–matter interaction, and without his deep insight, laid out convincingly in his memoir on our changing views of photons [25], we would never have accomplished the present work.

Author contribution

OB, JD and AK conceived the idea and the experiment. JRA, OB and BY analysed it theoretically. OB, TDB, DS and AH built the setup and performed the experiments. JRA, MIJ, OB and BY analysed experimental results. JRA, MIJ and AK wrote the manuscript with feedback from all authors.

Competing interests

The authors declare no competing interests.

Data availability statement

The data that support the findings of this study are openly available at the following URL/DOI: https://doi.org/10.5287/bodleian:dq9jJPxG5.

ORCID iDs

Juan-Rafael Álvarez https://orcid.org/0000-0003-3411-8237
Ben Yuen https://orcid.org/0000-0003-0430-4944
Thomas D Barrett https://orcid.org/0000-0001-6241-3028
Axel Kuhn https://orcid.org/0000-0002-5101-8732

References

[1] Schrödinger E 1935 *Naturwissenschaften* **23** 807
[2] Adlam E 2021 *Foundations of Quantum Mechanics* (*Elements in the Philosophy of Physics*) (Cambridge: Cambridge University Press)
[3] Landsman K 2017 *Foundations of Quantum Theory: From Classical Concepts to Operator Algebras* (*Fundamental Theories of Physics*) ed K Landsman (Berlin: Springer) pp 435–57
[4] Lloyd S 1997 arXiv:quant-ph/9703042
[5] Zhang J, Liu Y-x, Wu R-B, Jacobs K and Nori F 2017 *Phys. Rep.* **679** 1
[6] Habib S, Jacobs K and Mabuchi H 2002 *Science* **27** 126–35
[7] Yamamoto Y, Imoto N and Machida S 1986 *Phys. Rev.* A **33** 3243
[8] Armen M A, Au J K, Stockton J K, Doherty A C and Mabuchi H 2002 *Phys. Rev. Lett.* **89** 133602
[9] Smith W P, Reiner J E, Orozco L A, Kuhr S and Wiseman H M 2002 *Phys. Rev. Lett.* **89** 133601
[10] Sayrin C *et al* 2011 *Nature* **477** 73
[11] Zhou X, Dotsenko I, Peaudecerf B, Rybarczyk T, Sayrin C, Gleyzes S, Raimond J M, Brune M and Haroche S 2012 *Phys. Rev. Lett.* **108** 243602
[12] Legero T, Wilk T, Kuhn A and Rempe G 2003 *Appl. Phys.* B **77** 797
[13] Ollivier H *et al* 2021 *Phys. Rev. Lett.* **126** 063602
[14] Gao Y Y, Lester B J, Zhang Y, Wang C, Rosenblum S, Frunzio L, Jiang L, Girvin S and Schoelkopf R J 2018 *Phys. Rev.* X **8** 021073
[15] Woolley M J, Lang C, Eichler C, Wallraff A and Blais A 2013 *New J. Phys.* **15** 105025
[16] Mirza I M and van Enk S 2015 *Opt. Commun.* **343** 172
[17] Nisbet-Jones P B R, Dilley J, Holleczek A, Barter O and Kuhn A 2013 *New J. Phys.* **15** 053007
[18] Legero T, Wilk T, Kuhn A and Rempe G 2006 *Advances in Atomic, Molecular, and Optical Physics* vol 53 (Amsterdam: Elsevier) p 253

[19] Hong C K, Ou Z Y and Mandel L 1987 *Phys. Rev. Lett.* **59** 2044
[20] Kuhn A and Ljunggren D 2010 *Contemp. Phys.* **51** 289
[21] Nisbet-Jones P B R, Dilley J, Ljunggren D and Kuhn A 2011 *New J. Phys.* **13** 103036
[22] Vasilev G S, Ljunggren D and Kuhn A 2010 *New J. Phys.* **12** 063024
[23] Peruzzo A *et al* 2010 *Science* **329** 1500
[24] Barrett T D *et al* 2019 *Quantum Sci. Technol.* **4** 025008
[25] Shore B W 2020 *Our Changing Views of Photons: A Tutorial Memoir* 1st edn (Oxford: Oxford University Press)